Uncertainty Analysis of Experimental Discharge Coefficients in Additively Manufactured Liquid Injector Elements

James P. Venters,[1] Melissa Costa,[2] Evan C. Unruh,[3] David M. Lineberry,[4] and Robert A. Frederick[5]
The University of Alabama in Huntsville Propulsion Research Center, Huntsville, AL, 35899, USA

Jessica Wood,[6]
NASA Marshall Space Flight Center, Huntsville, AL, 35899, USA

James Hulka,[7]
Jacobs Technology, Inc., Jacobs Space Exploration Group, Huntsville, AL, 35899, USA

Screening of two additively manufactured liquid injector designs was conducted in the UAH high pressure spray facility. Four variants of each geometry with slightly different dimensions were obtained from eleven separate commercial additive manufacturing services. The devices were manufactured from Inconel 625 using the selective laser melting (SLM) powder bed process. The devices were cold flowed with water over a range of relevant pressure drops (75 psi to 1500 psi) to produce water flow rates from 0.037 to 1.75 lbm/s into ambient back pressure. Discharge coefficients determined from the testing along with the associated uncertainties provide insight into characteristic flow performance variabilities that can be expected from the SLM process for similar geometries.

I. Nomenclature

A_{throat} = smallest cross-sectional area in an injector flow path
$B_{P_{cal}}$ = systematic uncertainty of pressure transducer calibration
$B_{P_{repeat}}$ = repeatability of pressure transducer
$C_{d\ inj}$ = flow discharge coefficient of an injector
$C_{d\ vent}$ = Flow discharge coefficient of venturi flow meters
$N_{\dot{m}_{sample}}$ = number of samples taken at a mass flow set point
$N_{C_{d\ inj\ sample}}$ = number of samples taken at a mass flow set point
N_{sample} = number of samples taken at a set point
$N_{setpoint}$ = number of set points
P_{cav} = cavitation pressure
P_{in} = pressure into injector
S_P = random uncertainty of pressure measurement
$U_{\dot{m}_{setpoint}}$ = Uncertainty of mass flow set point
$U_{C_{d\ inj\ setpoint}}$ = Uncertainty of injector Cd at one set point
$U_{C_{d\ inj}}$ = Uncertainty of injector Cd
$U_{C_{d\ vent\ setpoint}}$ = Uncertainty of one set point in venturi calibration
$U_{C_{d\ vent\ setpoint}}$ = Uncertainty of venturi calibration set point

[1] Undergraduate Research Assistant, Mechanical and Aerospace Engineering Department, AIAA Student Member
[2] Undergraduate Research Assistant, Mechanical and Aerospace Engineering Department, AIAA Student Member
[3] Graduate Research Assistant, Mechanical and Aerospace Engineering Department, AIAA Student Member
[4] Research Engineer, Mechanical and Aerospace Engineering Department, AIAA Senior Member
[5] Professor, Mechanical and Aerospace Engineering Department, AIAA Associate Fellow
[6] Combustion Devices Engineer, Component Technology Branch, AIAA Senior Member
[7] Subject Matter Expert, Component Technology Branch, AIAA Associate Fellow

$U_{C_{d\ vent}}$ = Uncertainty of Venturi Cd
$U_{P_{95}}$ = Uncertainty of pressure transducer
U_m = Uncertainty of mass
U_t = Uncertainty of time
$U_{\Delta P}$ = Uncertainty of ΔP transducer
U_ρ = Uncertainty of density
d_1 = inside diameter of pipe before venturi
d_t = throat diameter
g_c = gravitational constant
$\dot{m}$ = mass flow rate
$t_{\alpha,\nu}$ = t- value
$\sigma_{\dot{m}_{sample}}$ = Standard deviation of all samples taken at a mass flow set point
$\sigma_{C_{d\ inj\ sample}}$ = standard deviation of all samples taken at a mass flow set point
$\sigma_{C_{d\ inj\ setpoint}}$ = standard deviation of all set points during injector test
$\sigma_{C_{d\ vent\ sample}}$ = Standard deviation of all samples taken at a set point in calibration
$\sigma_{C_{d\ vent\ setpoint}}$ = Standard deviation of all set points during calibration
A = cross-sectional area
C_d = flow discharge coefficient
ΔP = pressure differential
ρ = density
m = mass of water used in venturi catch and weigh calibration
t = time used in venture catch and weigh

II. Introduction

Additive manufacturing (AM), particularly the Selective Laser Melting **(**SLM) process, has received interest as a manufacturing method for fabricating intricate injectors. The capability of the process to reduce part count and labor costs is attractive. However, injectors with intricate geometries and small features generally require smooth surfaces which can be challenging to manufacture with the SLM process. Parts produced from the powder bed printing processes tend to exhibit flow behavior divergent from those produced with machining methods historically used for these parts. Therefore, there is a need for characteristic flow data collected from AM flow articles.

III. Experiment Setup and Methodology

Cold flow testing of each device was conducted in the UAH Propulsion Research Center high pressure spray facility. Tests were conducted using filtered, deionized water as the fluid simulant and were discharged into atmospheric back pressure. Single test runs sweeping from low pressure/low flow rate to high pressure/high flow rate were conducted on 11 test articles for each of four variants of two flow circuit designs. The primary measure of performance in the study was the discharge coefficient.

A. Test Article Design

The injector consisted of two separate flow circuit designs: a duct with a venturi restriction, and a radially-fed annulus. These geometries are shown in Figure 1. A test article for each flow circuit was fabricated with more traditional machining processes to serve as a baseline. Four variants of the two designs were developed, each with slight dimensional variations of critical geometries as summarized in Table 1. The variants of the designs were intended to provide insight into the sensitivity of flow behavior to geometric variations for additively manufactured flow articles. The four design variants were additively manufactured by eleven separate commercial vendors out of Inconel 625 using the SLM process. Each manufacturer printed the four variants on one build plate.

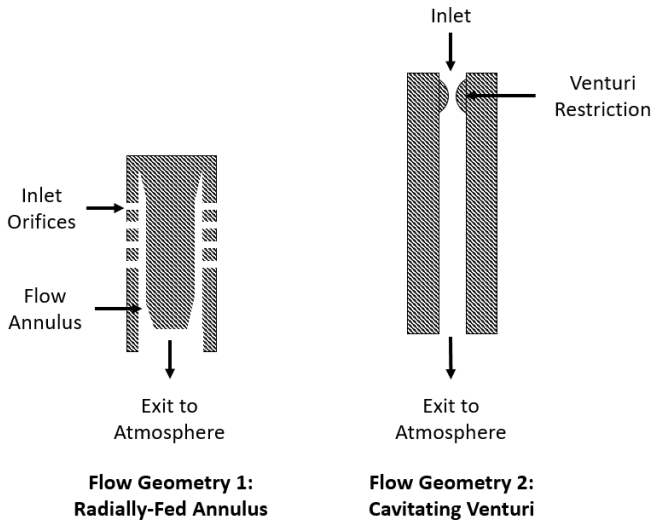

Figure 1: Test Article Design

Table 1: Test Article Design Dimensions

	Flow Geometry 1: Radially-Fed Annulus				Flow Geometry 2: Cavitating Venturi	
Design Variant	**Radial Hole ID (% of Baseline)**	**# of Radial Holes**	**Annulus ID (% of Baseline)**	**Annulus OD (% of Baseline)**	**Flow Duct ID (% of Baseline)**	**Venturi ID (% of Baseline)**
1	100	168	100	100	100	100
2	100	168	111.2	100	100	105.3
3	115.8	168	107.5	111.9	100	110.5
4	157.9	67	103.7	100	100	115.8
Baseline	100	168	100	100	100	100

B. Experimental Setup and Instrumentation

The Propulsion Research Center (PRC) high pressure spray facility was designed for the study of flow characteristics of full-scale injectors in an inert environment. The facility has the capability to produce up to 3 lbm/s of water flow rate either into a pressurized chamber (up to 500 psig) or at an atmospheric spray bench. The primary propellant simulant used in the facility is filtered and de-ionized water. The water is pressure fed from a 60 gal. run tank to either the pressurized chamber or the atmospheric spray station. The facility has high speed imaging capability as well as laser diagnostic capability.

For the current study, the facility was configured with the flow path shown in Figure 2 and Figure 3. A manifold was installed at the atmospheric spray bench to house the flow articles. Both circuits flow from the same main supply line, however only one circuit at a time was evaluated. This was accomplished using a three-way selector valve near the flow manifold. The water flow path contained two differential pressure venturi flowmeters installed in parallel in the system. The flow meters can be isolated via ball valves in order to cover a wide range of flow rates without modification to the flow path. Static pressure transducers were located at the inlet to the venturis and at the flow inlets of each leg of the manifold. A differential pressure transducer was located across the venturi. The supply pressure range selected for the flow annulus was from 75 to 550 psig. For the venturi, a pressure range of 50 to 1550 psig was selected. High speed imaging of the sprays was also obtained with the high-speed camera configuration as shown in Figure 4.

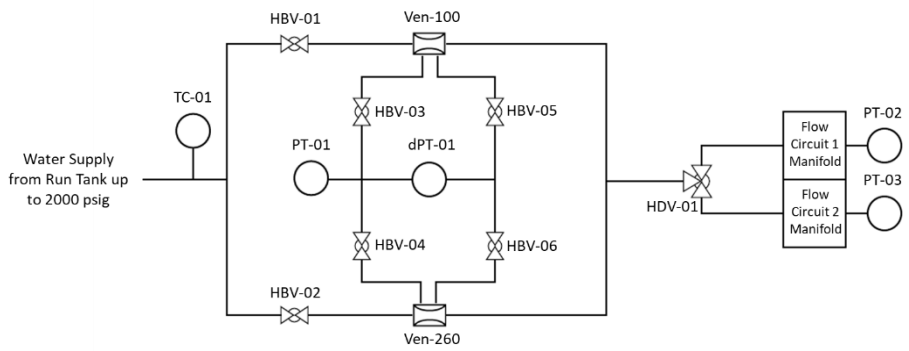

Figure 2: Experiment Flow Setup

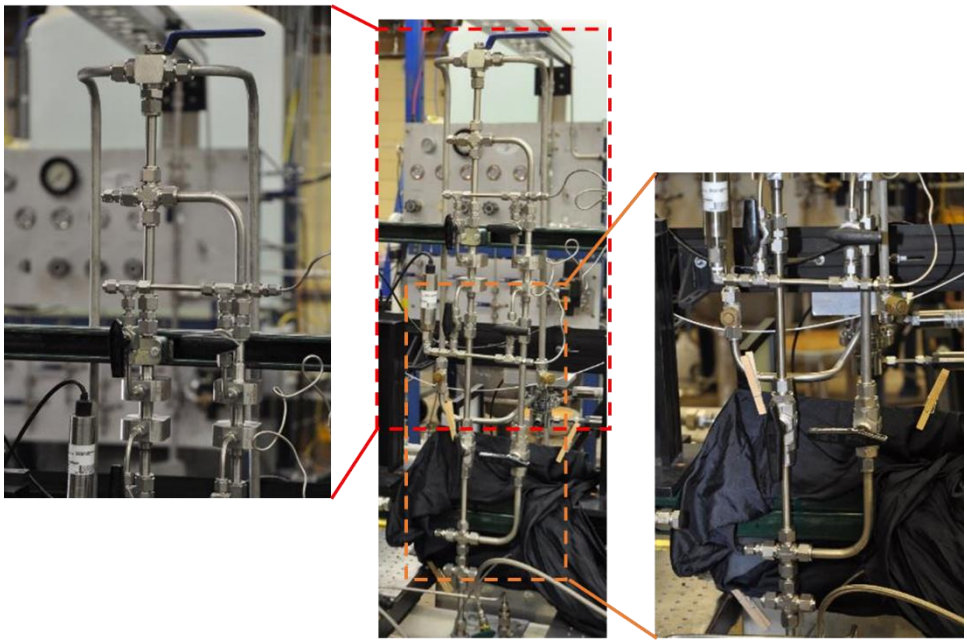

Figure 3: Flow Setup Installed in Facility

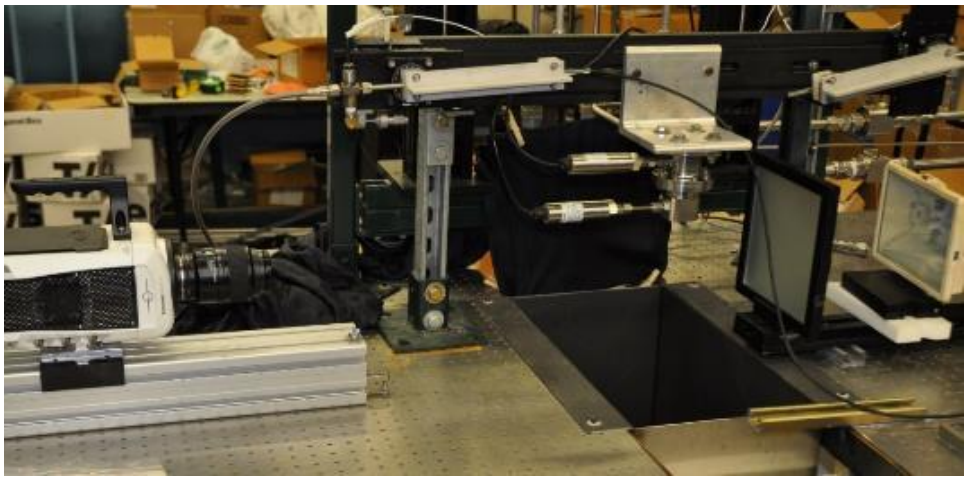

Figure 4: Setup with High Speed Camera

C. Uncertainty Analysis of Instrumentation

General uncertainty analysis of pressures and mass flow rates as collected by the instrumentation was performed using the Taylor Series Method (TSM). Pressures were collected with pressure transducers, for which the uncertainty can be estimated with Equation 1. [1]

$$U_{P_{95}} = \sqrt{{B_{P_{cal}}}^2 + {B_{P_{repeat}}}^2 + {S_P}^2} \tag{1}$$

where $U_{P_{95}}$ is the 95% uncertainty estimate for the pressure, $B_{P_{cal}}$ is the systematic uncertainty from the calibration of the pressure transducer which was determined from a linear regression uncertainty methodology as outlined in Coleman and Steel [1], $B_{P_{repeat}}$ is the repeatability of the transducer (0.2% FS = 0.2 psi), and S_P is the random uncertainty of the measurement (1.96σ).

Prior to testing, both of the differential pressure venturis were calibrated in place using a timed capture method. The calibration was performed at several different steady state flow rates using the same pressure transducer and same data acquisition system (DAQ) that were used for later flow testing of the injector test articles. Deionized water was flowed through the venturis and captured in a catch basin. The collection time was hand recorded with a stopwatch, and the differential pressure from the venturi was recorded on the DAQ. The mass collected divided by the collection time was then used to estimate the average mass flow rate through the venturi for a single calibration point. The discharge coefficient for a single calibration point for the venturi was then calculated according to the data reduction equation

$$C_{d\ vent} = \frac{\frac{m}{t}}{\sqrt{\frac{2\rho\Delta P}{\frac{1}{\left(\frac{\pi {d_t}^2}{4}\right)^2} - \frac{1}{\left(\frac{\pi {d_1}^2}{4}\right)^2}}}}, \tag{2}$$

where m is the mass of the water collected, t is the time of collection, ΔP is the pressure difference between the inlet and the throat of the venturi, ρ is the density of the fluid (water), d_t and d_1 are the diameters of the venturi throat and inlet respectively. Systematic uncertainty estimates for each of the parameters in Equation 2 are summarized in Table 2. The uncertainty in the mass collected mass, B_m, was taken as ½ of the resolution of the scale used to measure the mass. An estimate of 0.5s was taken as the uncertainty of the timing device and is considered a conservative estimate for human reaction time. The density uncertainty, B_ρ, was obtained from the NIST webbook for water density [2] using a range of expected values for temperature in the lab and pressures used during calibration. $B_{\Delta P}$ was obtained using Equation 1 above. Because the venturis did not change from test to test the diameters were constant. Thus, the uncertainty in these diameters was assumed to be negligible.

Table 2: Uncertainty Estimates for the Venturi C_d Data Reduction Equation

Parameter	95% Uncertainty Estimate
B_m	0.0025 lbm
B_t	0.5 s
B_ρ	0.0045 lbm/ft^3
$B_{\Delta P}$	1.17 psid

The uncertainty in the discharge coefficient at each calibration point was calculated as the sum of the squares of the systematic uncertainty associated with that calibration point and the random uncertainty for that calibration point according to

$$U_{C_{d\ vent\ setpoint}} = \sqrt{\left(B_{Cd\ vent\ setpoint}\right)^2 + \left(\frac{1.96\sigma_{C_{d\ vent\ sample}}}{\sqrt{N_{sample}}}\right)^2}. \tag{3}$$

An estimate for the random uncertainty was taken as the standard deviation of the value of Cd calculated at each pressure measurement in the data set divided by the square root of the number of samples in the data set and multiplied by a confidence value to provide 95% confidence. The systematic uncertainty, $B_{Cd\ vent\ setpoint}$, was calculated using a generalized uncertainty methodology for propagation of errors. Using the data reduction equation for Cd defined by equation 2, systematic uncertainty is calculated as

$$B_{C_{d\ vent\ setpoint}} = \sqrt{\left(\frac{\partial C_{d\ vent}}{\partial m}B_m\right)^2 + \left(\frac{\partial C_{d\ vent}}{\partial t}B_t\right)^2 + \left(\frac{\partial C_{d\ vent}}{\partial \rho}B_\rho\right)^2 + \left(\frac{\partial C_{d\ vent}}{\partial \Delta P}B_{\Delta P}\right)^2} \tag{4}$$

and the partial derivatives are calculated as [1]

$$\frac{\partial C_{d\ vent}}{\partial m} = \frac{2\sqrt{2}}{{d_1}^2{d_t}^2\pi\sqrt{\frac{\Delta P\rho}{{d_1}^4-{d_t}^4}t}} \tag{5}$$

$$\frac{\partial C_{d\ vent}}{\partial t} = \frac{-2m\sqrt{2}}{{d_1}^2{d_t}^2\pi t^2\sqrt{\frac{\Delta P\rho}{{d_1}^4-{d_t}^4}}} \tag{6}$$

$$\frac{\partial C_{d\ vent}}{\partial \rho} = \frac{-m\sqrt{2}}{{d_1}^2{d_t}^2\pi t\sqrt{\frac{\Delta P\rho}{{d_1}^4-{d_t}^4}}} \tag{7}$$

$$\frac{\partial C_{d\ vent}}{\partial \Delta P} = \frac{-m\sqrt{2}}{\Delta P{d_1}^2{d_t}^2\pi m\sqrt{\frac{\Delta P\rho}{{d_1}^4-{d_t}^4}}} \tag{8}$$

The discharge coefficients at each steady state calibration point were averaged to determine a single C_d for each venturi. The uncertainty for the average C_d was then calculated using,

$$U_{C_{d\ vent}} = \sqrt{\sum\left(\frac{U_{C_{d\ vent\ setpoint}}}{N_{setpoint}}\right)^2 + \left(\frac{t_{\alpha,\nu}*\sigma_{C_{d\ vent}}}{\sqrt{N_{setpoint}}}\right)^2} \tag{9}$$

where $N_{setpoint}$ is the number of calibration setpoints, t was acquired from a standard t-value chart at 95% uncertainty [1] with $\nu = N_{setpoint} - 1$. Using the outlined methodology, the discharge coefficients for the two venturis were determined to be 1.02 ± 0.03 and 0.98 ±.05. These values are in line with expectations from the manufacturer. Values greater than 1 are an indication that there are either bias uncertainties in the instrumentation used for the calibration, or that the actual values of constants (density or diameters) could be slightly different than the values used for analysis.

With uncertainty for the venturi discharge coefficients determined, the mass flow rate as determined by using these venturis is then calculated according to the data reduction equation

$$\dot{m} = \frac{\pi}{4}C_{d\ vent}\ {d_t}^2\sqrt{\frac{2\rho\Delta P}{1-(\frac{{d_t}^4}{{d_1}^4})}} \tag{10}$$

where the variables are as they have already been defined. The uncertainty in a new mass flow rate is calculated according to

$$U_{\dot{m}_{setpoint}} = \sqrt{\left(\frac{\partial \dot{m}}{\partial C_{d\ vent}}U_{C_{d\ vent}}\right)^2 + \left(\frac{\partial \dot{m}}{\partial \rho}U_\rho\right)^2 + \left(\frac{\partial \dot{m}}{\partial \Delta P}U_{\Delta P}\right)^2 + \left(\frac{1.96\sigma_{\dot{m}_{sample}}}{\sqrt{N_{\dot{m}_{sample}}}}\right)^2} \tag{11}$$

with the partial derivative terms in equation (11) becoming

$$\frac{\partial \dot{m}}{\partial C_{d\,vent}} = \frac{{d_1}^2 {d_t}^2 \pi \sqrt{\frac{2\Delta P \rho}{{d_1}^4 - {d_t}^4}}}{4} \tag{12}$$

$$\frac{\partial \dot{m}}{\partial \rho} = \frac{C_{d\,vent} {d_1}^2 {d_t}^2 \Delta P \pi \sqrt{2}}{8({d_1}^4 - {d_t}^4)\sqrt{\frac{\Delta P \rho}{{d_1}^4 - {d_t}^4}}} \tag{13}$$

$$\frac{\partial \dot{m}}{\partial \Delta P} = \frac{C_{d\,vent} {d_1}^2 {d_t}^2 \pi \sqrt{2} \rho}{8({d_1}^4 - {d_t}^4)\sqrt{\frac{\Delta P \rho}{{d_1}^4 - {d_t}^4}}} \tag{14}$$

IV. Flow Test Results

For each design element, flow data was collected at steady state conditions at set inlet pressures moving from low to high pressures. The resulting mass flow rates were collected with the inlet pressures. Data was collected at 1000 Hz for approximately ten seconds of steady flow at each set point. Each set pressure was selected to be sufficiently high to ensure cavitation in the injector flow circuits. Although each of the Manufacturers printed all four of the design elements, a couple of the elements had blocked passages or were broken during transport or post processing, therefor some of the design variants have fewer than eleven test articles. A sample of the steady state mass flow and inlet pressure for geometry 1, design variant 1 is shown in Figure 5. While most of the test articles showed a consistent trend between mass flow and inlet pressure, a few of the test articles had some unexpected behavior. The one notable exception on Figure 5 is the data for manufacturer 11. This dataset shows a distinct stepped increase in mass flow around an inlet pressure of 325 psi. It is believed that step was most likely due obstruction in the element flow path, possibly from leftover powder material. The increase in mass flow is likely a result of the obstruction becoming dislodged. In instances like this, the later data was assumed to best characterize the trends and the lower pressure data was neglected for the analysis.

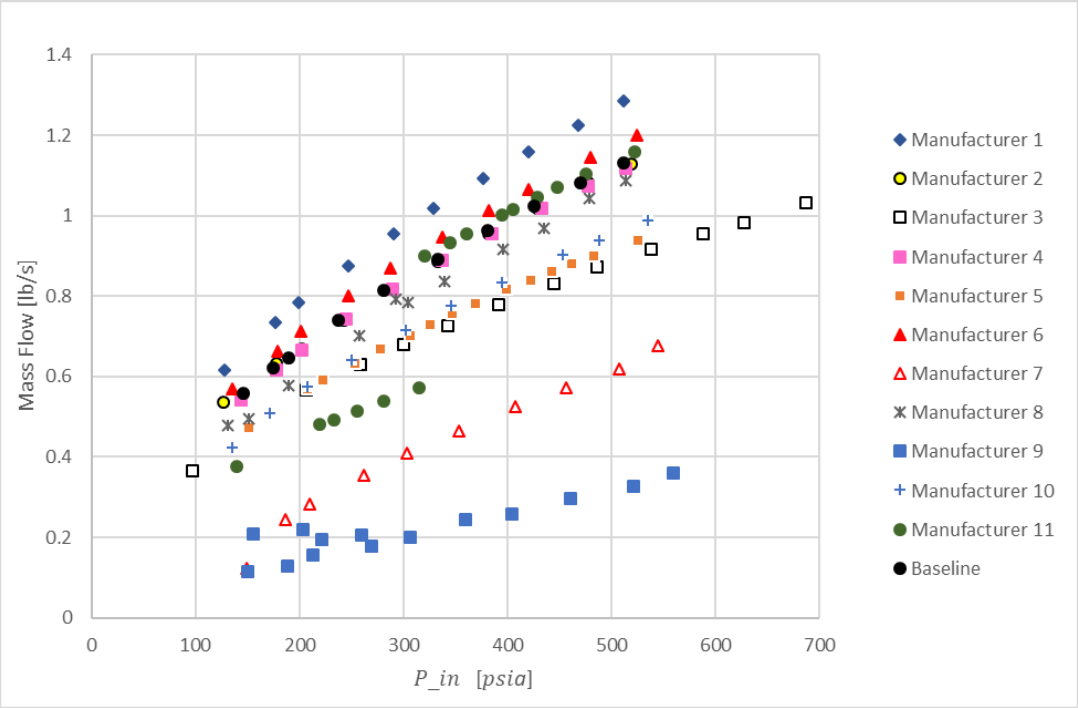

Figure 5: Flow Geometry 1, Design Variant 1, Mass Flow vs Pressure

A cavitating flow article with a discharge coefficient that is constant with pressure will exhibit a linear relationship between mass flow and the square root of the difference in pressure between the inlet pressure and the cavitation pressure. Plotting the collected mass flow rate vs the square root of pressure difference for each inlet pressure set point of a given test article allows one to evaluate the consistency of the test article's discharge behavior over a range of pressures. If the data shows a nearly linear relationship, then the discharge coefficient can be approximated as a constant with respect to pressure. Figure 6 shows this plot for the first test article at each set point. Additional plots for the remaining test articles can be found in Appendix A. These plots show that, for the range of inlet pressures tested, the discharge behaviors of the injectors can be described with constant Cd values.

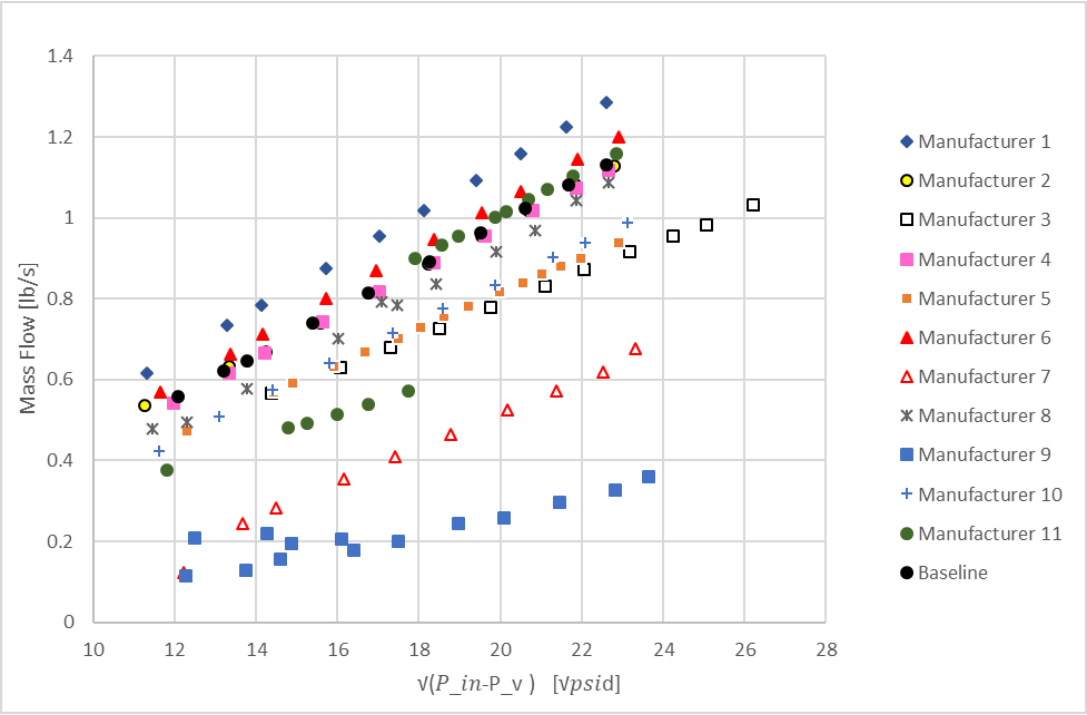

Figure 6: Flow Geometry 1, Design Variant 1, Mass Flow Correlation

V. Analysis of Results

The pressure and mass flow rate results were used along with the design dimensions of the test articles to calculate C_d values for each design geometry. Uncertainty analysis was performed for the calculated C_d values, then a statistical analysis of the resulting C_d values and uncertainties was performed to gain insight into the flow performance of the each additive flow geometry/design variant population based on the results of the sample tests.

A. Calculation and Uncertainty of Discharge Coefficients

With the mass flow rate determined from Equation 10, the discharge coefficient for the injectors was found using Equation 15. The non-dimensional discharge coefficient was used to compare each of the articles of the same design across all manufacturers.. For each flow geometry investigated, the data reduction equation for discharge coefficient of that element, $C_{d\ inj,}$ was calculated as the average of the Cd values for that element at each setpoint, $C_{d\ inj\ setpoint}$. For these calculations, Equation 2 was used with the assumptions that $d_1 >> d_2$, thus $1/d_1$ was approximately zero and that the flow was cavitating, thus the throat pressure is equal to cavitation pressure. With these assumptions, the equation for C_d becomes [3]

$$C_d = \frac{\dot{m}}{A_{throat}\sqrt{2\rho(P_{in}-P_{cav})}}, \tag{15}$$

and the associated uncertainty is calculated by combining the systematic uncertainties associated with mass flow, density and inlet pressure and the random uncertainty associated with the steadiness of the setpoint according to

$$U_{C_d} = \sqrt{\left(\frac{\partial C_{d\,inj}}{\partial \dot{m}} B_{\dot{m}}\right)^2 + \left(\frac{\partial C_{d\,inj}}{\partial \rho} B_{\rho}\right)^2 + \left(\frac{\partial C_{d\,inj}}{\partial P_{in}} B_{P_{in}}\right)^2 + \left(\frac{1.96\sigma_{C_d}}{\sqrt{N_{C_d}}}\right)^2}. \quad (16)$$

The partial derivatives in Equation 16 with respect to each variable can be found as

$$\frac{\partial C_d}{\partial \dot{m}} = \frac{1}{A_{throat}\sqrt{2\rho(P_{in}-P_{cav})}} \quad (17)$$

$$\frac{\partial C_d}{\partial \rho} = \frac{-0.5\dot{m}}{\rho A_{throat}\sqrt{-2\rho(P_{cav}-P_{in})}} \quad (18)$$

$$\frac{\partial C_d}{\partial P_{in}} = \frac{-\sqrt{2}*\dot{m}}{4(P_{in}-P_{cav})A_{throat}\sqrt{\rho(P_{in}-P_{cav})}} \quad (19)$$

where ṁ is acquired from Equation 10, A_{throat} is the smallest area in the flow circuit,and the density value, ρ, *was* acquired from the NIST webbook [2] P_{in} is the inlet pressure measured through the DAQ. The water vapor pressure, P_{cav} was assumed to be constant. For each setpoint, a value of C_d was calculated at each set of measured parameters in the data set. The standard deviation of these Cd values multiplied by a confidence factor, 1.96 for 95% confidence, and divided by the number of samples, N_{C_d} represents the random uncertainty of the setpoint. Since the DAQ takes samples at 1000 Hz,N for each set point is on the order of thousands and the last term in Equation 16 typically was very small relative to the systematic uncertainty terms. The Cd values calculated for each measurement in the dataset are averaged to determine the discharge coefficient for a single geometry/design variant of a single manufacturer at a single setpoint. These Cd values were denoted as $C_{d\,inj\,setpoint}$. The average of the Cd values for all setpoints of a single geometry/design variant of a single manufacturer were then averaged in order to acquire a single value for a single geometry/design variant of a single manufacturer, denoted as $C_{d\,inj}$. [1]

Finally, the uncertainty of the injector Cd can be found as

$$U_{C_{d\,inj}} = \sqrt{\sum\left(\frac{U_{C_{d\,inj\,setpoint}}}{N_{setpoint}}\right)^2 + \left(\frac{t_{\alpha,\nu}\,\sigma_{C_{d\,inj\,setpoint}}}{\sqrt{N_{setpoint}}}\right)^2} \quad (20)$$

where the first term of Equation 20 captures the uncertainty calculated for the Cd value determined at each setpoint in the data set,$N_{setpoint}$ is the number of test setpoints for a single manufacturer, $N_{setpoint}$, ranged from 9 to 15. $C_{d\,inj}$ is the average of $C_{d\,inj\,setpoint}$. $t_{\alpha,\nu}$ is acquired from a standard t value chart at 95% uncertainty and $\alpha = N_{setpoint} - 1$. [1] A sample plot of the discharge coefficients for geometry 1, design variant 1 is shown in Figure 7. For this configuration, the spread of the Cd values was, in general, wider than the uncertainty associated with the Cd value for each test article, with two of the test articles having Cd values significantly lower than the other nine. Plots for the remaining design variants are provided in Appendix B.

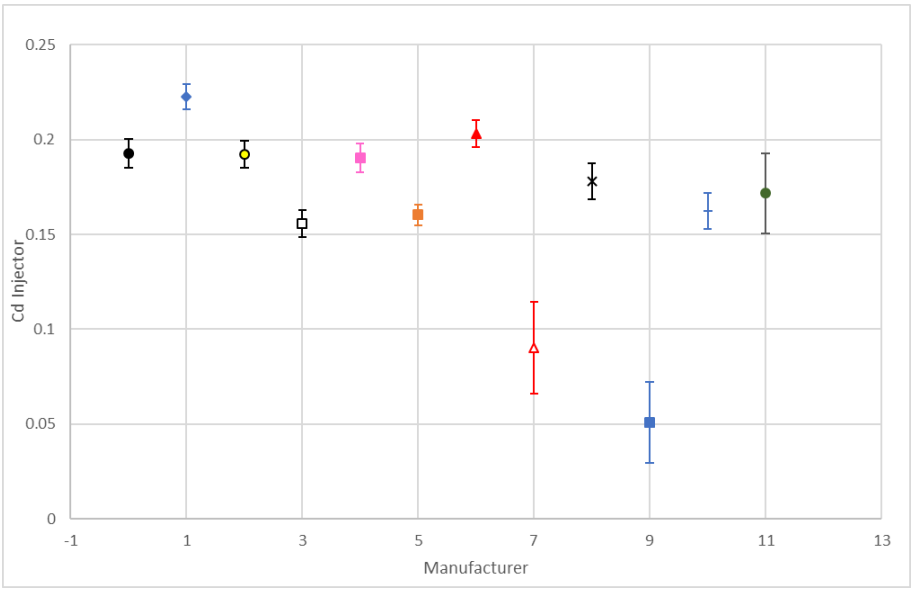

Figure 7: Discharge Coefficient values for geometry 1, design variant 1 for each manufacturer

B. Statistical Analysis of Discharge Coefficients

A statistical analysis of the results was performed to provide relevant statistics for the measured values and uncertainties of the discharge coefficients for the flow geometries investigated. Statistics investigated included sample means and variances for each design, as well as a 95% confidence interval for the C_d population mean.

For each of design variants of each geometry, a mean discharge coefficient $\overline{C_d}$ was calculated from the $C_{d\ inj}$ values for each manufacturer. The uncertainty for the average value was calculated using a variation of Equation 20 as denoted by

$$U_{\overline{C_d}} = \sqrt{\sum \left(\frac{U_{C_{d\ inj}}}{N}\right)^2 + \left(\frac{t_{\alpha,\nu}\,\sigma_{C_{d\ inj}}}{\sqrt{N}}\right)^2} \tag{21}$$

where N is the number of manufacturers for that particular design variant. These values are reported in Table 3 along with the upper and lower uncertainties on the standard deviations, which were found using

$$U_{\sigma\ upper} = \frac{(n-1)\left(\frac{U_{C_{d\ inj}}}{t_{cd}}\right)^2}{\chi^2_{1-\alpha/2,n-1}} \tag{22}$$

$$U_{\sigma\ lower} = \frac{(n-1)\left(\frac{U_{C_{d\ inj}}}{t_{cd}}\right)^2}{\chi^2_{\alpha/2,n-1}} \tag{23}$$

In Equations 22 and 23, U_σ is the uncertainty of the standard deviation. N is the number of samples for a given geometry and flow path. χ is from a Chi squared distribution chart. [4]

Table 3 shows a summary of the figures in Appendix B. Where results are separated by design variant and flow geometry. Mean Cd injector is the average Cd across all manufacturers. Uncertainty of mean Cd injector was calculated using a variation of Equation 20 where manufacturer is substituted for set point. Standard deviation is the standard deviation of mean Cd injector. Upper uncertainty of standard deviation was calculated using Equation 22. Lower uncertainty of standard deviation was calculated using Equation 23. Figure 8 shows the average Cd across all manufacturers for a given design variant and flow geometry

Table 3: Statistical Analysis of Results by Design Variant

Flow Geometry	Design Variant	Mean Cd Injector	Uncertainty of Mean Cd Injector	Standard Deviation	Upper Uncertainty of Standard Deviation	Lower Uncertainty of Standard Deviation
1	1	0.164	0.024	0.049	3.31E-04	5.77E-05
	2	0.158	0.023	0.043	3.55E-04	5.04E-05
	3	0.128	0.016	0.028	1.71E-04	2.13E-05
	4	0.176	0.018	0.032	1.99E-04	2.83E-05
2	1	0.815	0.078	0.127	3.75E-03	5.95E-04
	2	0.807	0.065	0.100	2.78E-03	3.95E-04
	3	0.783	0.051	0.077	1.81E-03	2.25E-04
	4	0.784	0.067	0.110	3.11E-03	3.87E-04

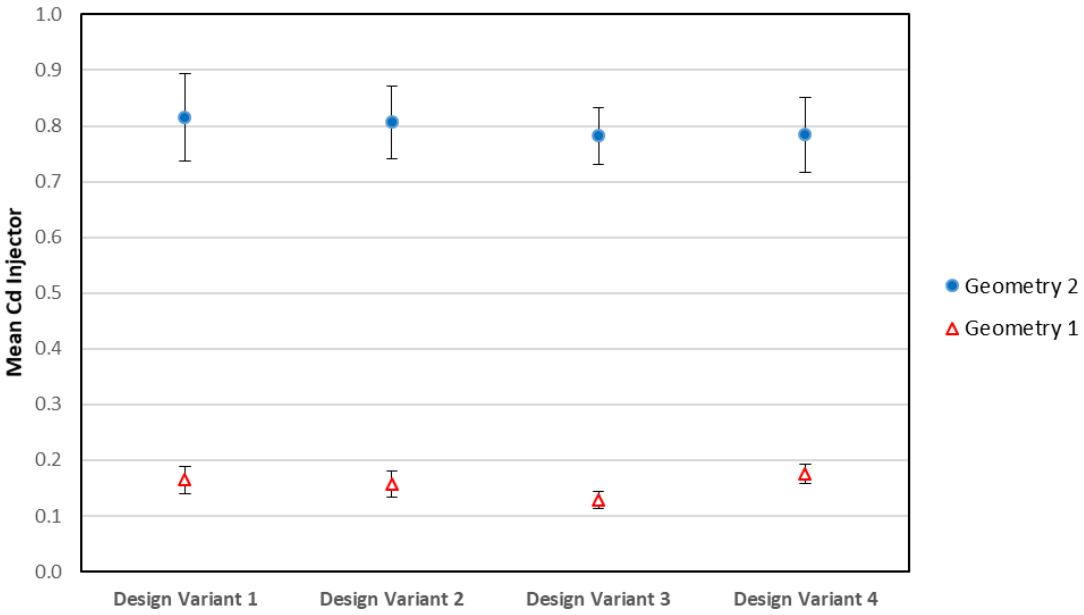

Figure 8: Statistical Analysis of Results by Design Variant

Although each design variant had slightly different features, all four design variants for each geometry should produce flow characteristics similar to the baseline geometries. The data shown on Figure 8 confirm that the mean values for each design variant for each of the two geometry are in fairly good agreement. As a method to compare the individual manufacturers, the average Cd of all design variants of each geometry produced by each manufacturer ware calculated. Uncertainties for these Cd values were calculated using Equation 21. Additionally, the standard deviation of Cd for each geometry of each manufacturer along with the upper and lower uncertainties of the standard deviation were calculated. Table 4 provides the results of this analysis and Figure 9 shows a plot of the mean Cd values for both geometries for all eleven manufacturers. Assuming that the additive test articles should match the baseline flow characteristics, the Cd values were normalized by the Cd for the baseline geometry, and that data is shown in Figure 10. As can be seen in this figure, the spread of the mean Cd values for geometry 1 was greater than that of geometry 2. It was expected that, because the complexity and geometric scales of geometry 1 relative to geometry 2, geometry 1 would be more difficult to additively manufacture. However, the normalized Cd values show that for eight of the manufacturers, the normalized Cd values for geometry 1 and geometry 2 were in very close agreement with each other, e.g. for manufacturer 1, the mean Cd values for both geometries were around 1.03, and for

manufacturer 6 the mean Cd values for both geometries were around 0.83. This may indicate that the skill level of the manufacturer and/or capabilities of the printers could be equally significant factors in the quality of these printed test articles as the part complexity.

Table 4: Statistical Analysis of Results by Manufacturer

Flow Geometry	Manufacturer	Mean Cd Injector	Uncertainty of Mean Cd Injector	Standard Deviation	Upper Uncertainty of Standard Deviation	Lower Uncertainty of Standard Deviation
1	Baseline	0.193	0.008	-	-	-
	1	0.203	0.030	0.024	1.94E-03	1.31E-05
	2	0.187	0.014	0.010	4.17E-04	2.83E-06
	3	0.150	0.038	0.036	1.08E-03	2.54E-05
	4	0.181	0.030	0.028	6.76E-04	1.59E-05
	5	0.144	0.024	0.022	4.18E-04	9.83E-06
	6	0.162	0.044	0.041	1.44E-03	3.39E-05
	7	0.122	0.037	0.033	9.82E-04	2.31E-05
	8	0.187	0.020	0.018	2.92E-04	6.88E-06
	9	0.086	0.053	0.042	5.98E-03	4.05E-05
	10	0.126	0.030	0.025	6.84E-04	1.61E-05
	11	0.169	0.024	0.021	1.95E-03	1.08E-06
2	Baseline	0.941	0.078	-	-	-
	1	0.962	0.061	0.018	7.98E-03	5.41E-05
	2	0.864	0.043	0.016	4.04E-03	2.74E-05
	3	0.747	0.050	0.041	1.84E-03	4.33E-05
	4	0.755	0.119	0.102	1.04E-02	2.45E-04
	5	0.662	0.036	0.017	9.71E-04	2.29E-05
	6	0.784	0.050	0.006	1.88E-03	4.41E-05
	7	0.855	0.044	0.011	1.45E-03	3.41E-05
	8	0.863	0.059	0.041	2.53E-03	5.96E-05
	9	-	-	-	-	-
	10	0.661	0.067	0.027	3.30E-03	7.78E-05
	11	0.824	0.033	0.012	3.70E-03	2.05E-06

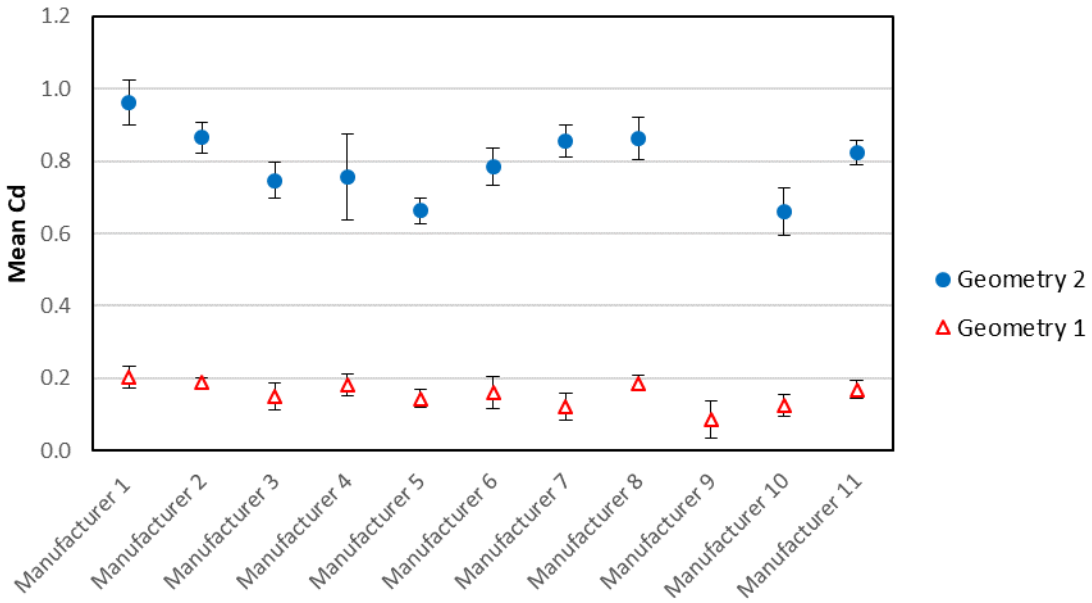

Figure 9 Comparison of Design variant mean Cd values for each geometry across all Manufacturers

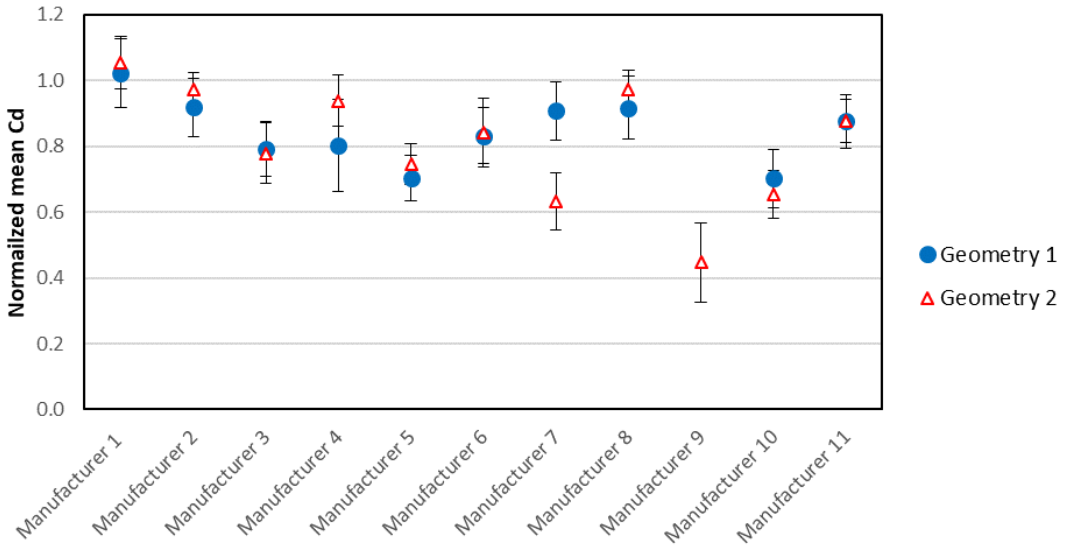

Figure 10: Comparison of Design variant mean Cd values for each geometry normalized by the baseline geometry Cd across all Manufacturers

C. Discharge Coefficient Prediction Interval for an Additional Manufacturer

Assuming that all additive manufacturing services are part of the same statistical population of the sample set of manufacturers used to fabricate the test articles in this investigation, the results of the statistical analysis of the injector discharge coefficients can be used to find a prediction interval for an expected Cd value for an additional manufacturer. [4] The prediction interval can be found using

$$C_{d_{Predicted}} = \overline{C_d} \pm U_{95}\sqrt{1+\frac{1}{n}} \tag{24}$$

where $\overline{C_d}$ is the average discharge coefficient between the collected manufacturers for a given design variant, n is the number of manufacturers used to find $\overline{C_d}$, and U_{95} is found using

$$U_{95} = \sqrt{\Sigma \left(\frac{U_{C_{d\,inj}}}{N}\right)^2 + \left(t_{\alpha,\nu}\, \sigma_{C_{d\,inj}}\right)^2} \tag{25}$$

Equation 25 is similar to Equation 21, except that the second term in the equation is no longer divided by the square root of the number of samples. Equation 25 represents the range of Cd values in which a new test article may be expected, and not the range in which the true mean of the population would be expected to fall.

The resulting expected value range can be plotted with the average Cd value and uncertainty of the average along with each of the injector Cd values as shown in Figure 11 for the first design variant. Additional variants are plotted in Appendix B. Table 5 shows the uncertainty and prediction interval for all flow geometries and design variants. The results of the prediction interval analysis indicate that for flow Geometry 1, the expected range of Cd values for a new element could vary from ±42% to ±68% of the mean value. For flow geometry 2, the prediction interval was lower ranging from ±24% to ±37% of the mean value.

Table 5: Prediction Intervals for Design Variants

Flow Geometry	Design Variant	Mean Cd Injector	Uncertainty of Mean Cd Injector	Prediction Interval
1	1	0.1642	± 0.0236	± 0.1117
	2	0.1577	± 0.0233	± 0.1020
	3	0.1280	± 0.0158	± 0.0672
	4	0.1757	± 0.0175	± 0.0753
2	1	0.8154	± 0.0778	± 0.2989
	2	0.8071	± 0.0653	± 0.2418
	3	0.7825	± 0.0512	± 0.1903
	4	0.7839	± 0.0672	± 0.2691

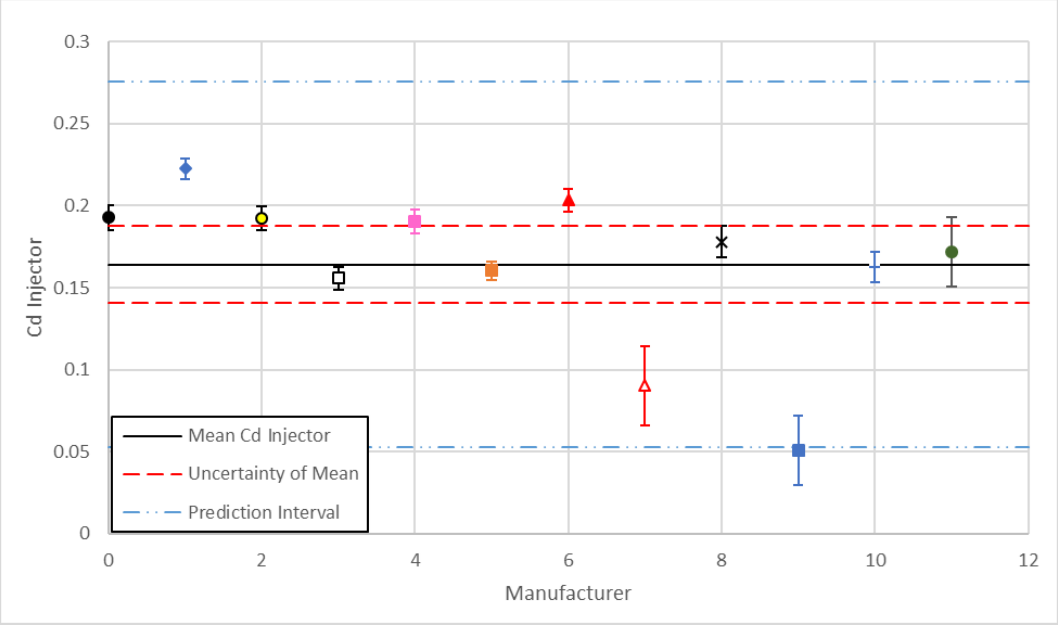

Figure 11: Flow Geometry 1, Design Variant 1, $C_{d\,inj}$ Summary

VI. Conclusion

Four variants of two injector flow geometries were additively manufactured by eleven different commercial 3D printing services using SLM powder-bed printers. The injector test articles were cold-flow tested with deionized water to determine cavitating discharge behaviors over a range of inlet pressures. The resulting datasets were reduced to an average discharge coefficient value for each test article. And a mean discharge coefficient for each design variant. Finally, the statistics as found from the selected sample set of test articles were used to find a discharge coefficient prediction interval for additional injector samples.

The uncertainty analysis of the testing demonstrates that the total uncertainties of the experimentally obtained Cd values are sufficiently low to positively distinguish differences in discharge behaviors between test articles. The variation in Cd values for each design variant of geometry 1 were significantly higher than those of geometry 2. This increased variation is likely due to a number of contributing factors which may include the complexity and scale of the geometric features, variations in the manufacturing processes, the build orientation, as well as capabilities of the manufacturer.

The statistical analysis of the discharge coefficients provides insight into the repeatability and state of the art SLM 3D printing as applied to geometries for combustion devices. This prediction interval can be used to predict a range of Cd values that injectors of similar geometries to those investigated and obtained from a manufacturer using similar SLM printing technology would be expected to fall. For this data the predication intervals ranged from ±42% to ±68% of the population mean value for geometry 1 and from ±24% to ±37% of the population mean value for geometry 2. These ranges seem very large relative to what may be expected from more traditional subtractive machining processes. While this range for the prediction interval is relevant for geometries with features of similar geometric scale and complexity, it is not expected that larger features would exhibit the same range of variation.

VII. References

[1] H. W. Coleman and W. G. Steele, Experiment Validation, and Uncertainty Analysis for Engineers, Wiley, 2018.

[2] National Institute of Standards and Technology, [Online]. Available: https://webbook.nist.gov/chemistry/fluid/. [Accessed 8 July 2019].

[3] ASME PTC 19.5-2004, The American Society of Mechanical Engineers, 2004.

[4] D. C. Montgomery and G. C. Runger, Applied Statistics and Probability for Engineers, Wiley, 2014.

VIII. Appendix A

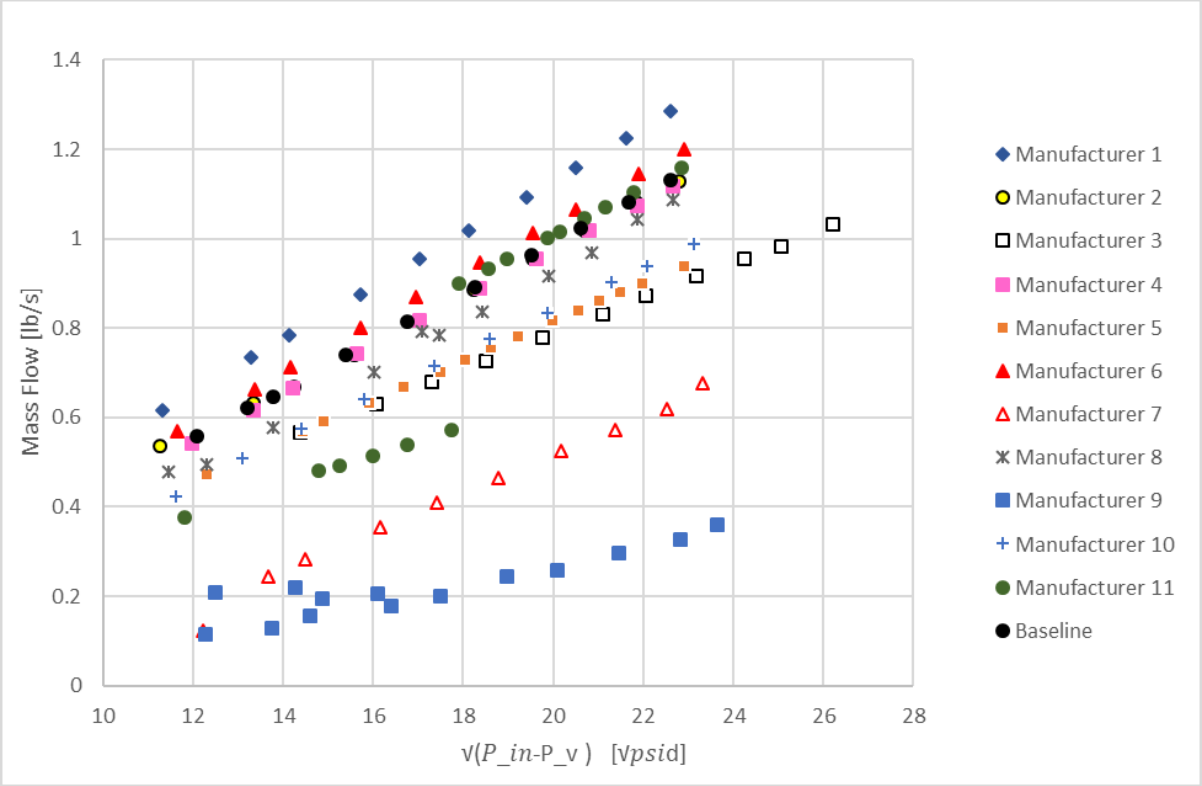

Figure A.1: Flow Geometry 1, Design Variant 1, Mass Flow Correlation

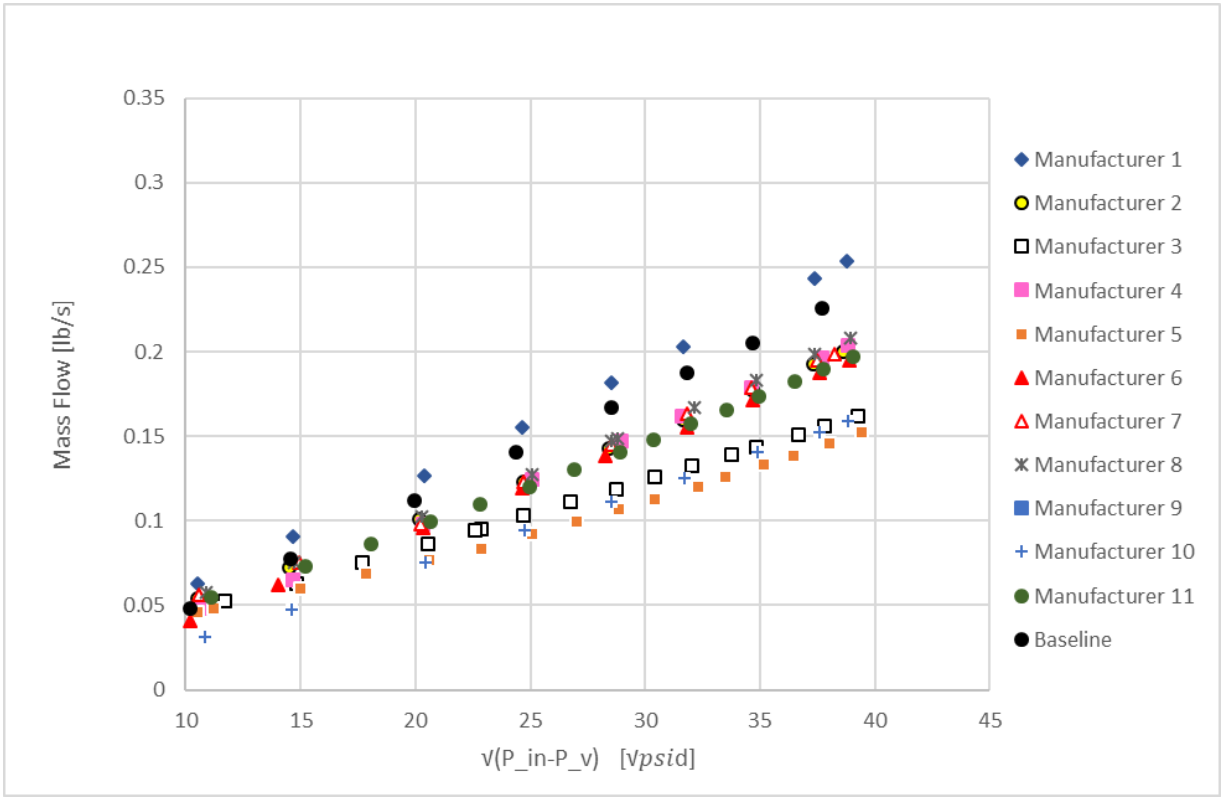

Figure A.2: Flow Geometry 2, Design Variant 1, Mass Flow Correlation

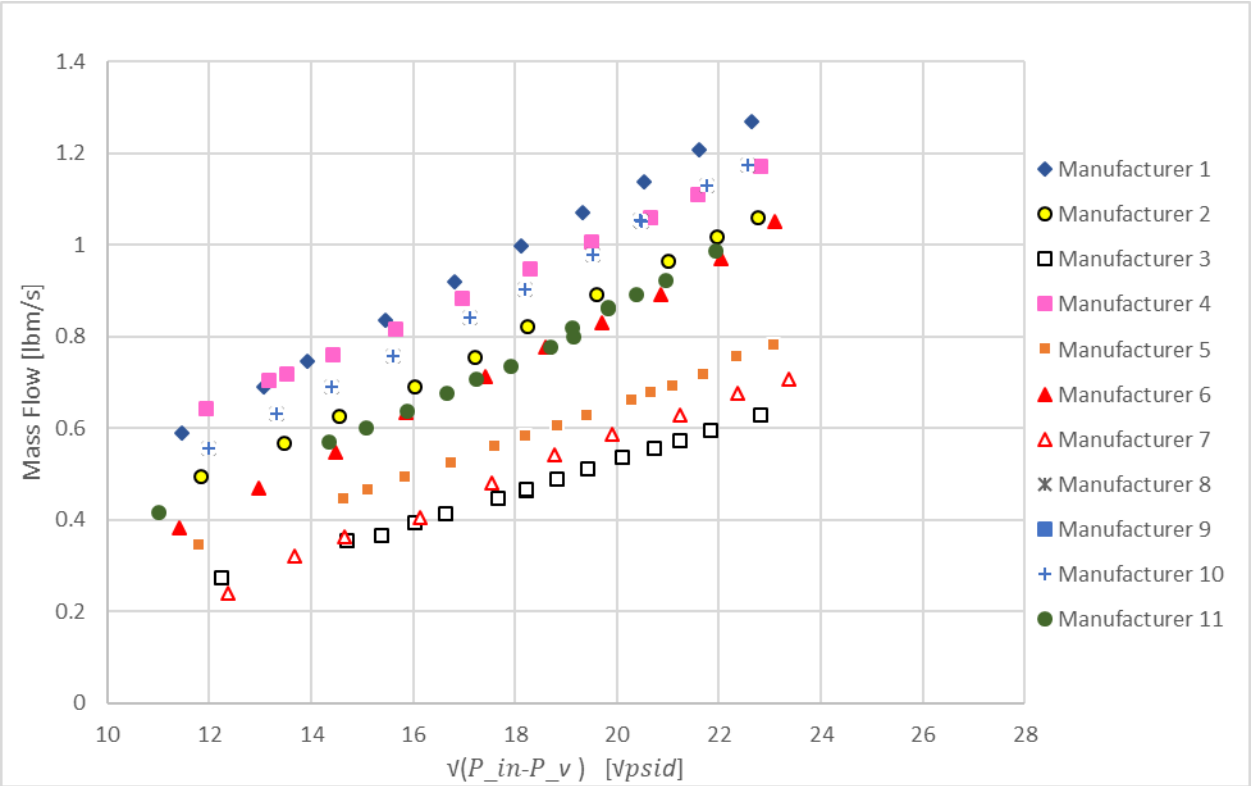

Figure A.3: Flow Geometry 1, Design Variant 2, Mass Flow Correlation

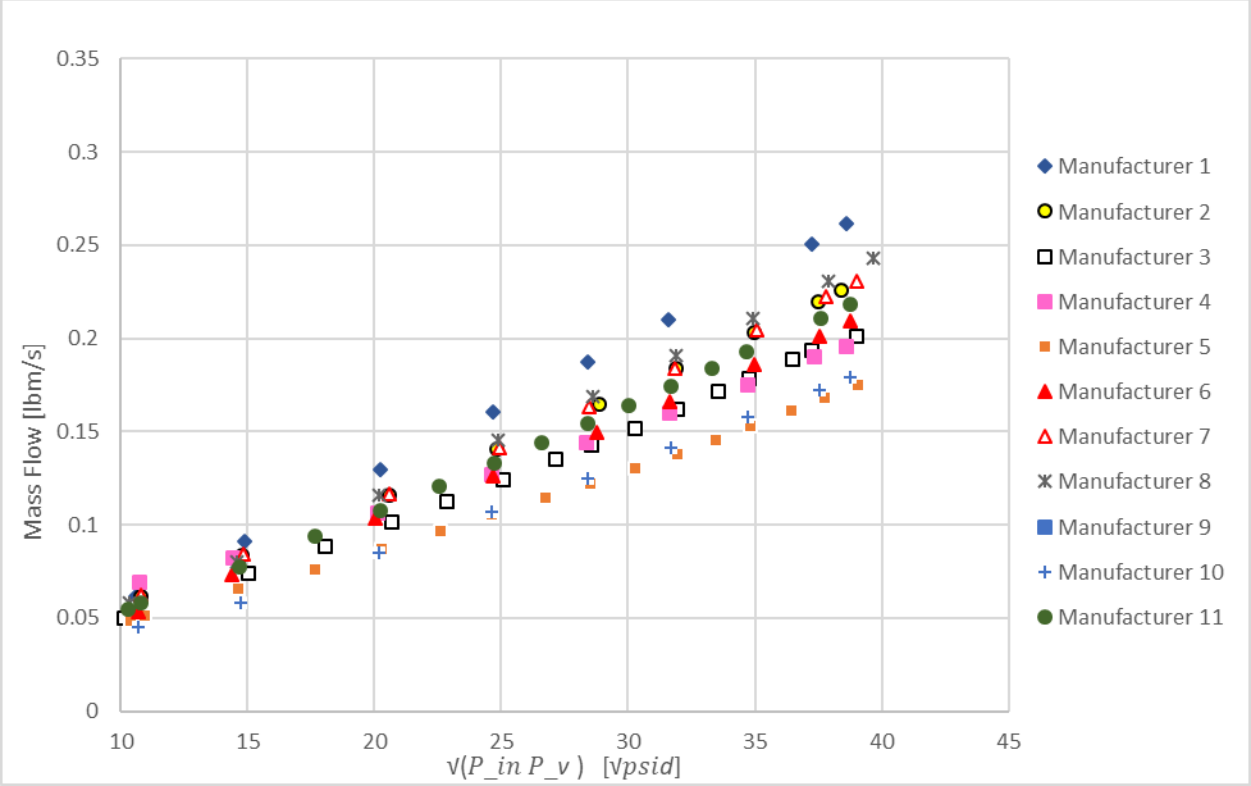

Figure A.4: Flow Geometry 2, Design Variant 2, Mass Flow Correlation

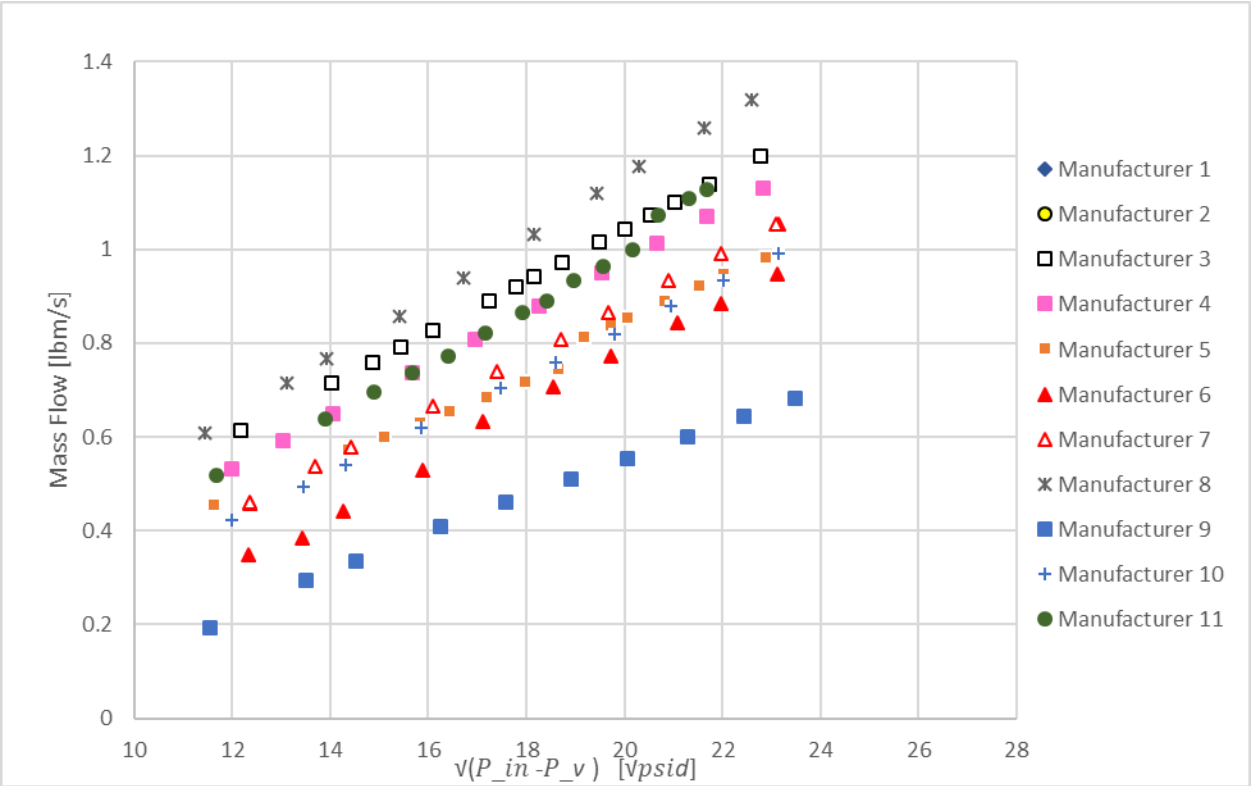

Figure A.5: Flow Geometry 1, Design Variant 3, Mass Flow Correlation

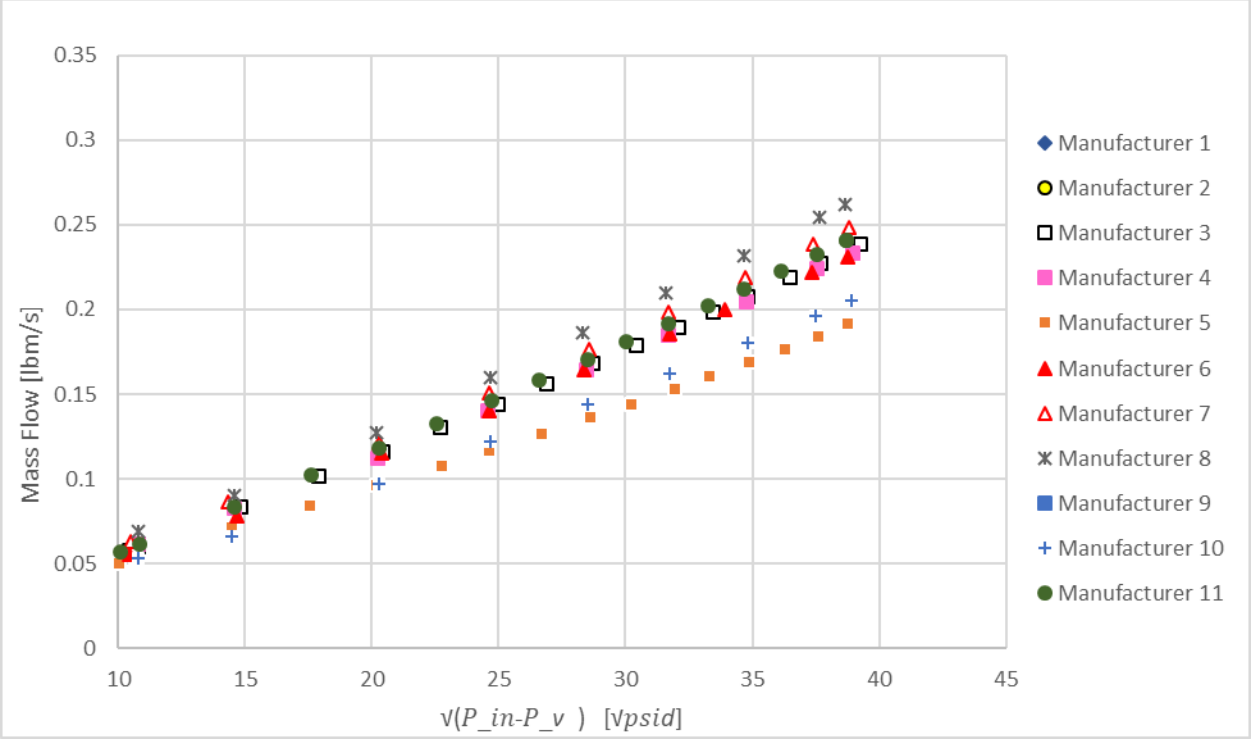

Figure A.6: Flow Geometry 2, Design Variant 3, Mass Flow Correlation

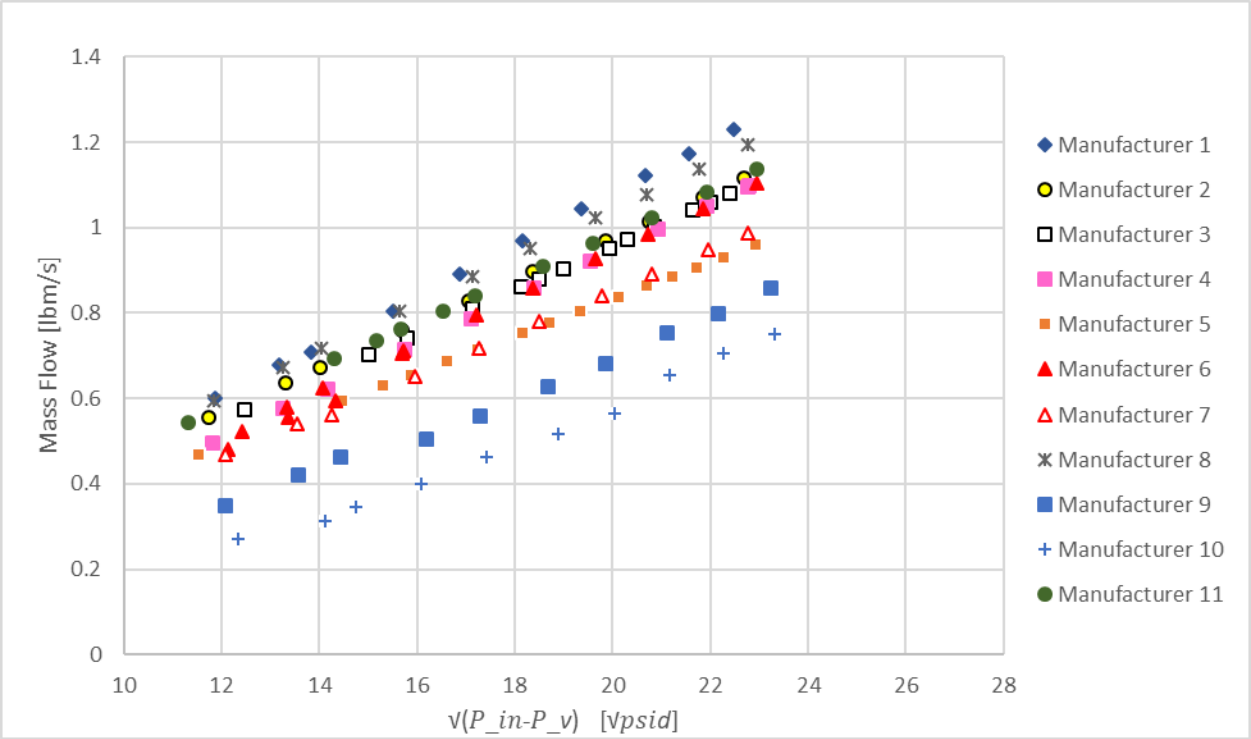

Figure A.7: Flow Geometry 1, Design Variant 4, Mass Flow Correlation

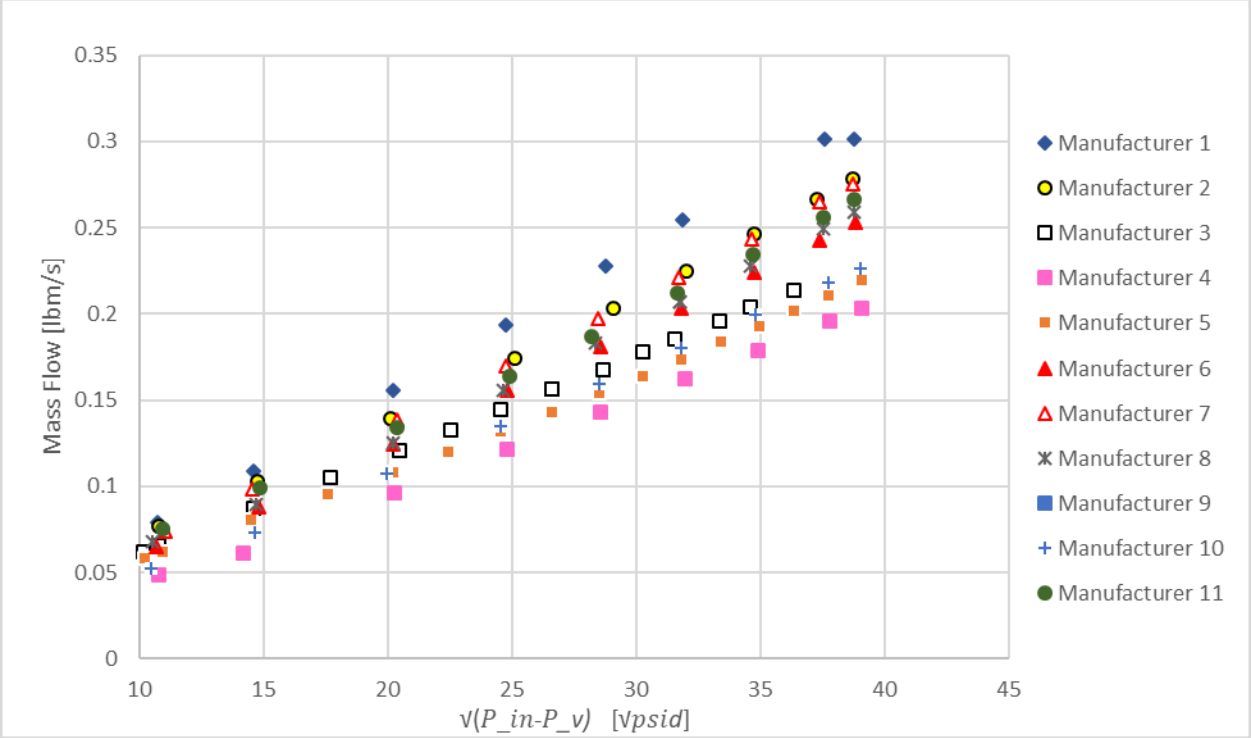

Figure A.8: Flow Geometry 2, Design Variant 4, Mass Flow Correlation

IX. Appendix B

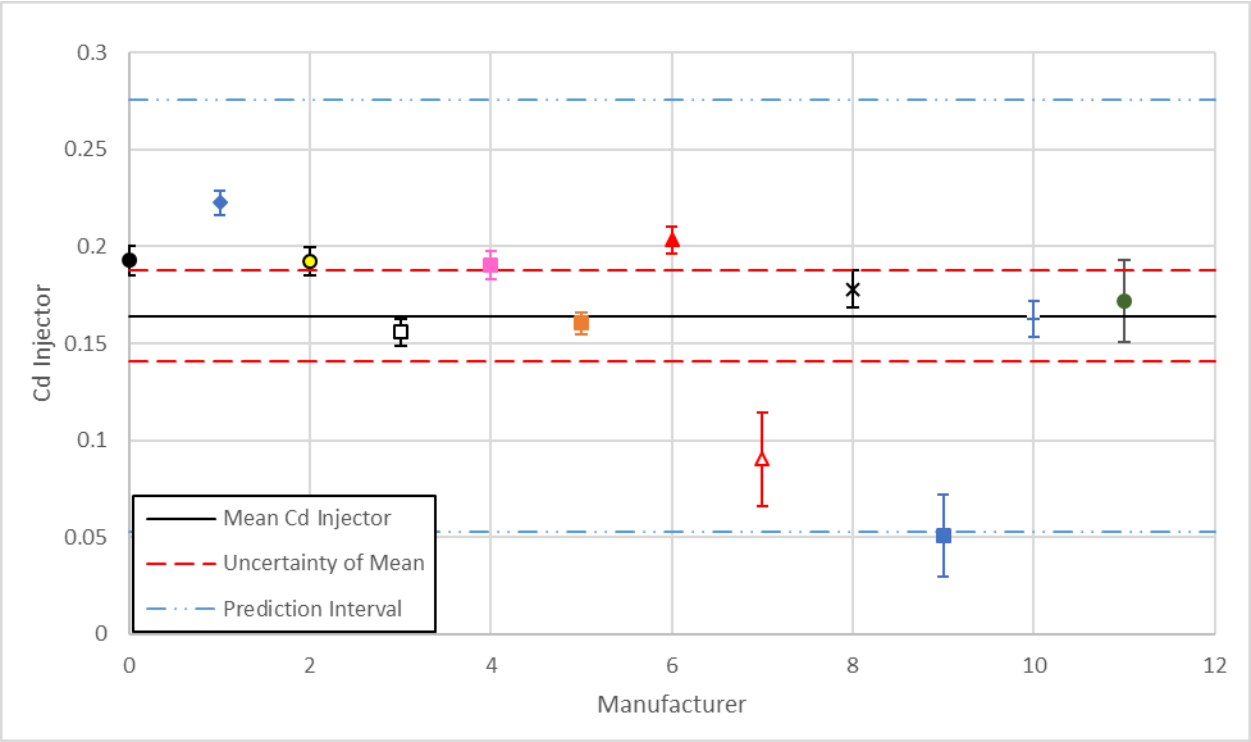

Figure B.1: Flow Geometry 1, Design Variant 1, $C_{d\ inj}$ Summary

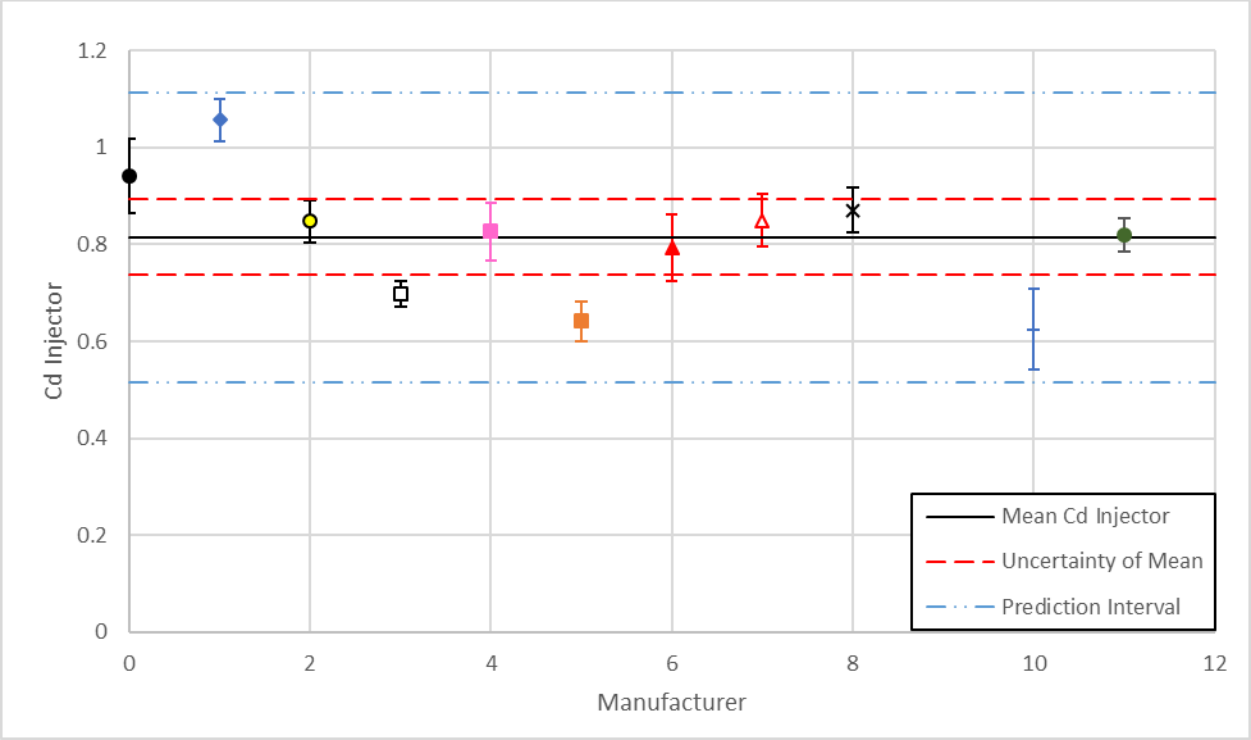

Figure B.2: Flow Geometry 2, Design Variant 1, $C_{d\ inj}$ Summary

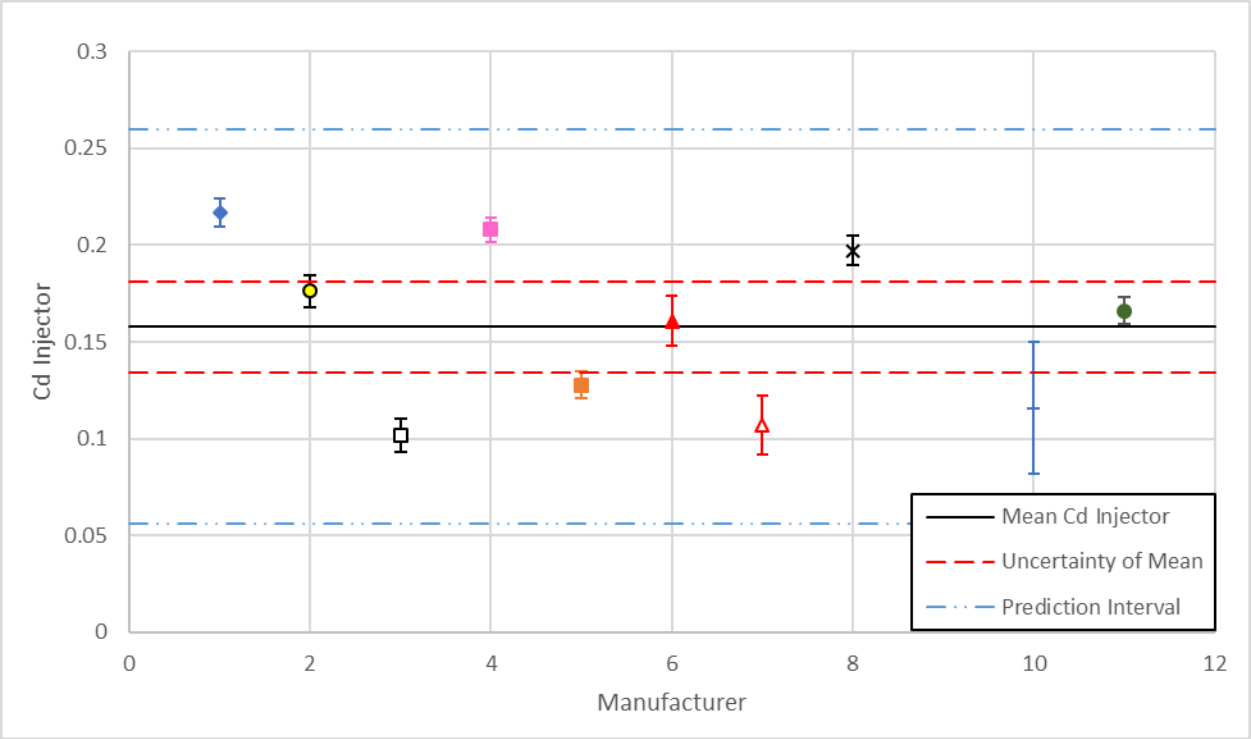

Figure B.3: Flow Geometry 1, Design Variant 2, $C_{d\ inj}$ Summary

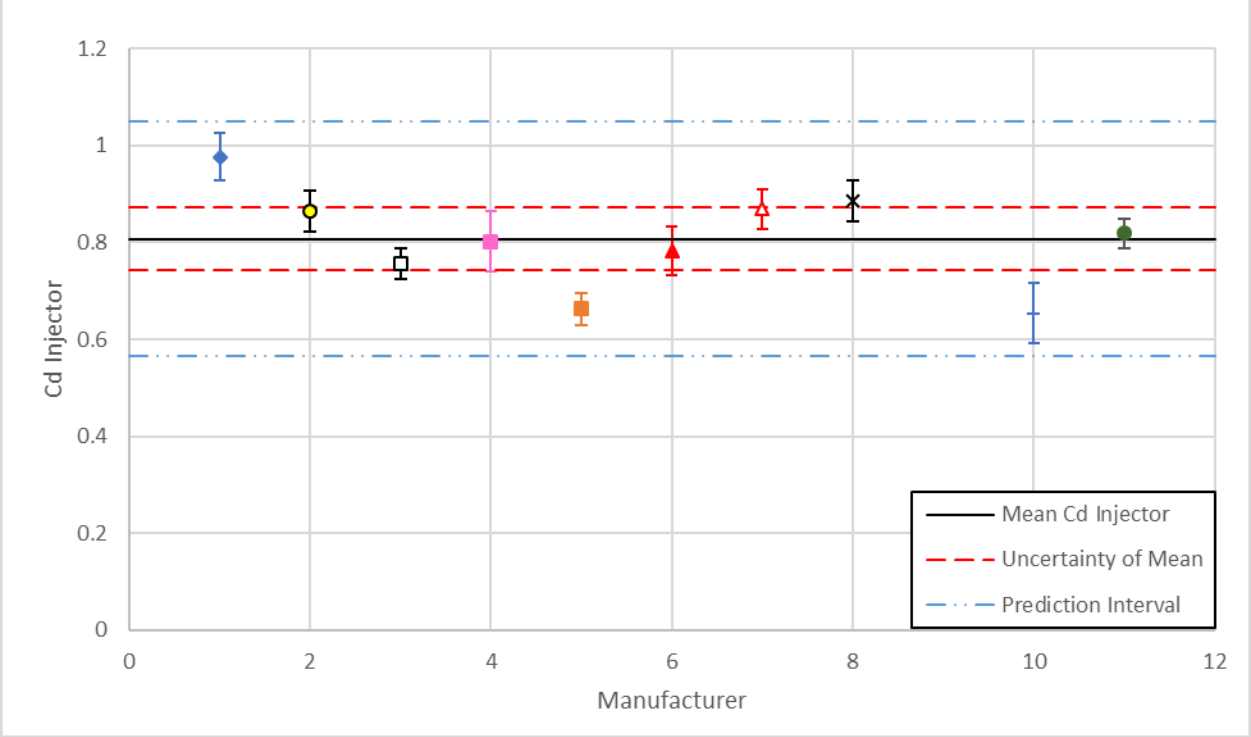

Figure B.4: Flow Geometry 2, Design Variant 2, $C_{d\ inj}$ Summary

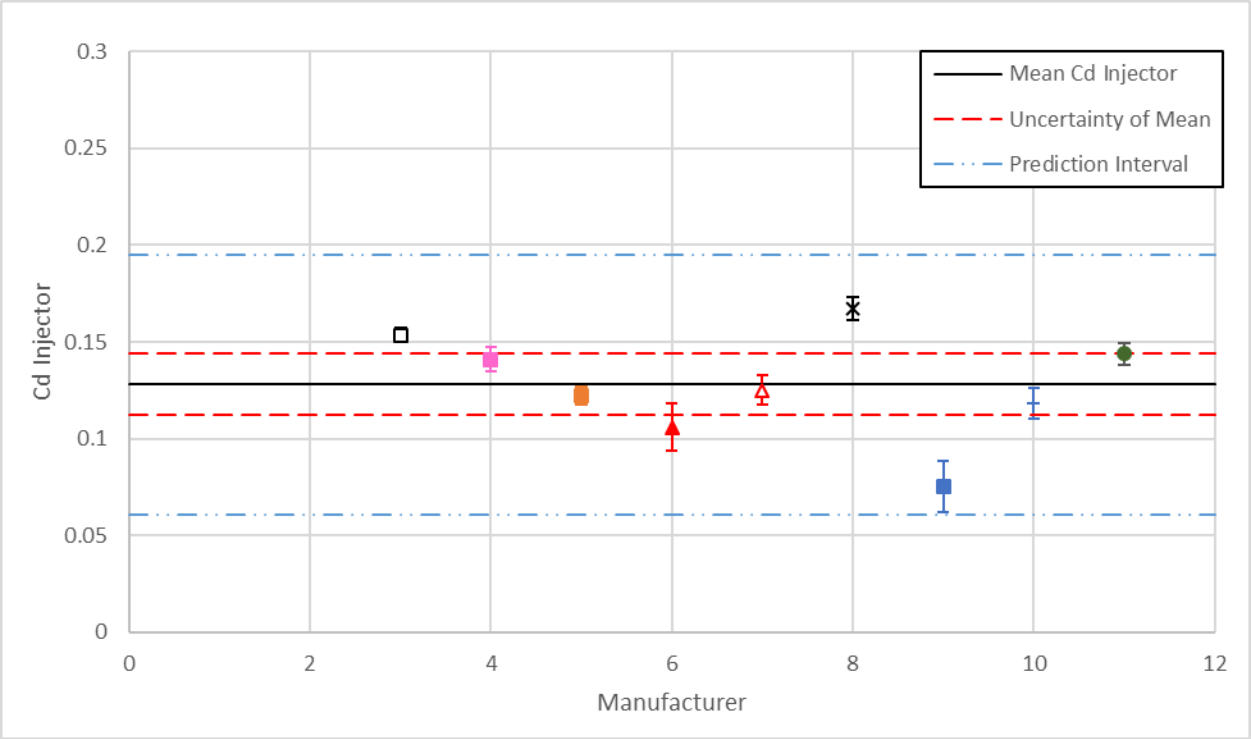

Figure B.5: Flow Geometry 1, Design Variant 3, $C_{d\,inj}$ Summary

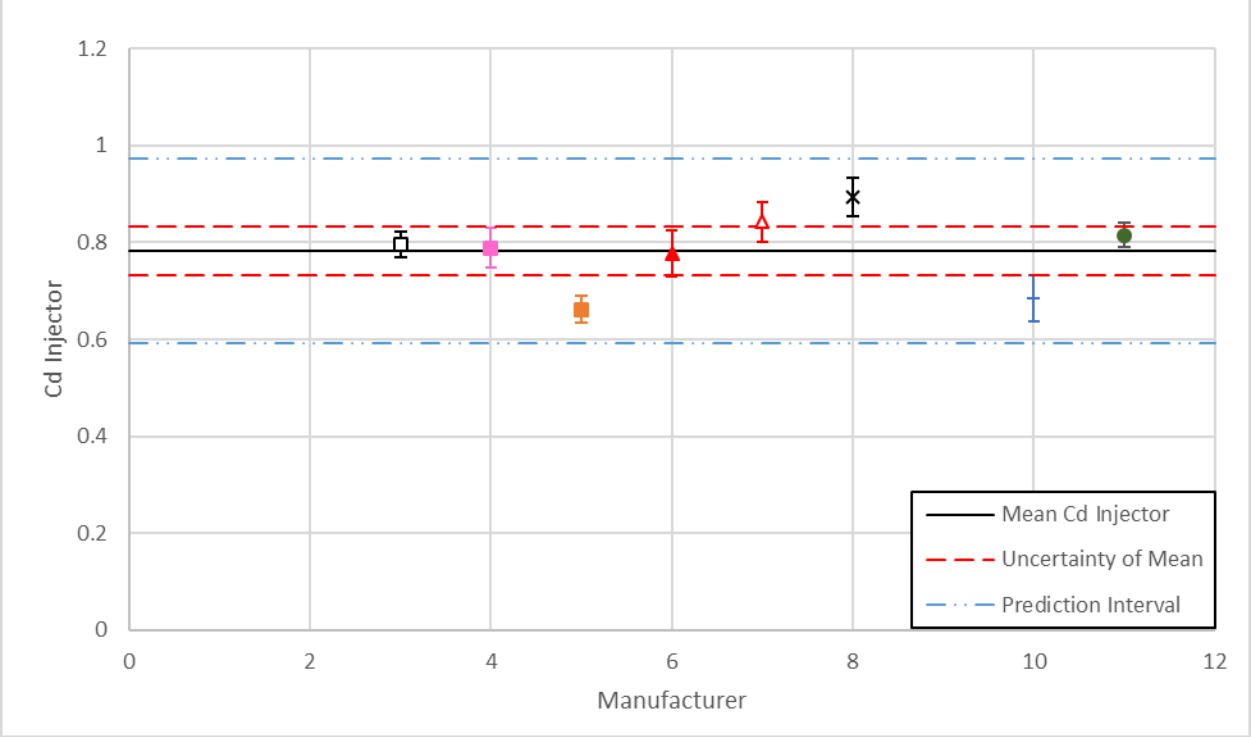

Figure B.6: Flow Geometry 2, Design Variant 3, $C_{d\,inj}$ Summary

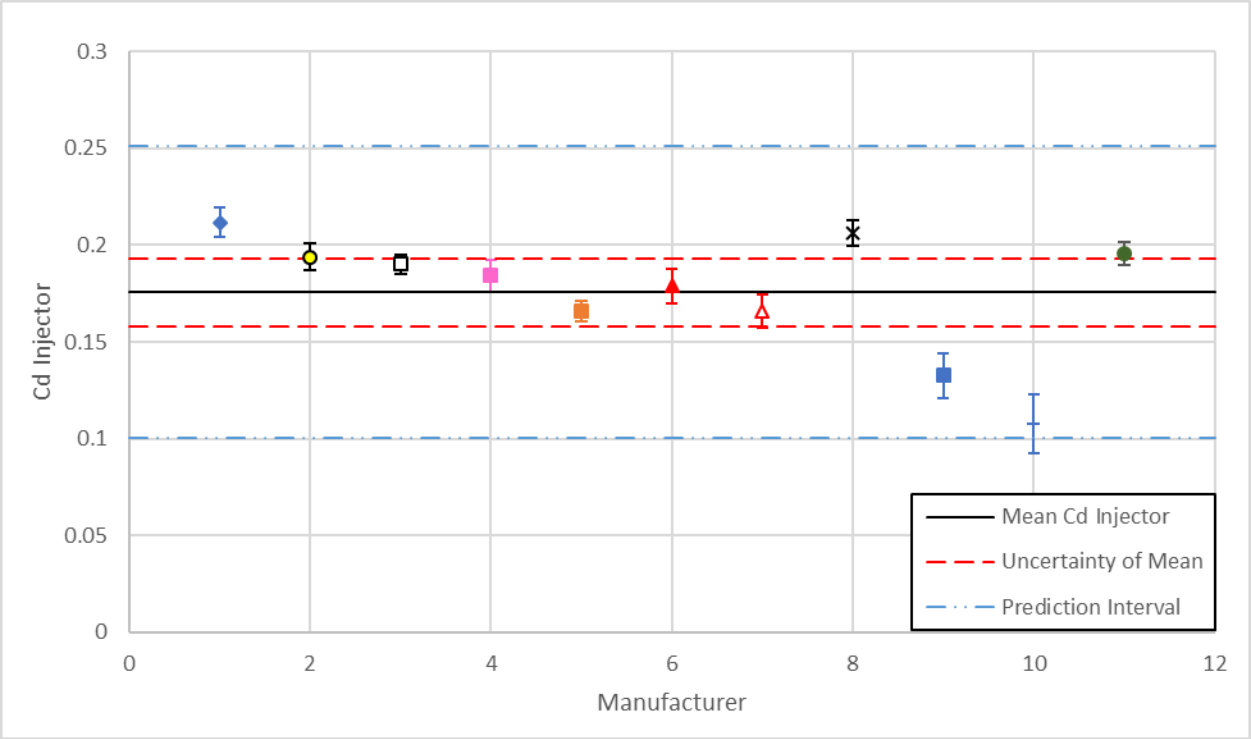

Figure B.7: Flow Geometry 1, Design Variant 4, $C_{d\,inj}$ Summary

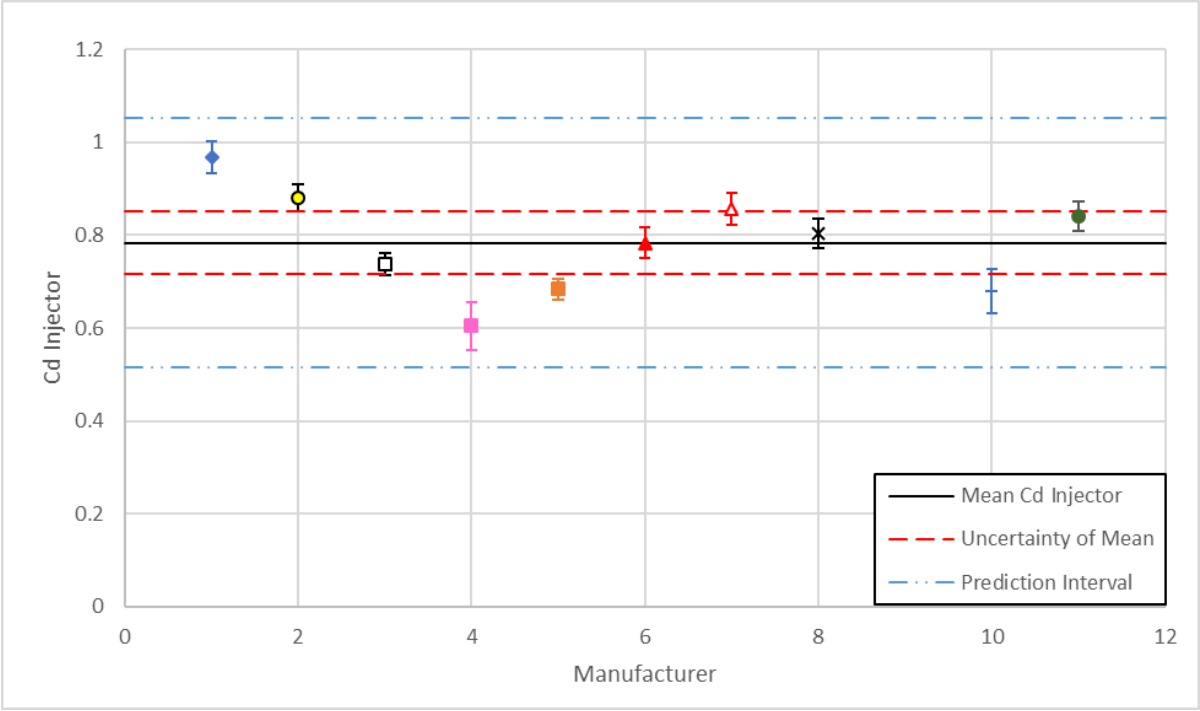

Figure B.8: Flow Geometry 2, Design Variant 4, $C_{d\,inj}$ Summary